

**Metal-Organic Cages**
How to cite: *Angew. Chem. Int. Ed.* **2023**, *62*, e202301612

International Edition: doi.org/10.1002/anie.202301612

German Edition: doi.org/10.1002/ange.202301612

# A Double-Walled Tetrahedron with $\text{Ag}^{\text{I}}$ Vertices Binds Different Guests in Distinct Sites\*\*

Samuel E. Clark, Andrew W. Heard, Charlie T. McTernan, Tanya K. Ronson, Barbara Rossi, Petr Rozhin, Silvia Marchesan,\* and Jonathan R. Nitschke\*

**Abstract:** A double-walled tetrahedral metal-organic cage assembled in solution from silver(I), 2-formyl-1,8-naphthyridine, halide, and a threefold-symmetric triamine. The  $\text{Ag}^{\text{I}}_4\text{X}$  clusters at its vertices each bring together six naphthyridine-imine moieties, leading to a structure in which eight tritopic ligands bridge four clusters in an  $(\text{Ag}^{\text{I}}\text{X})_4\text{L}_8$  arrangement. Four ligands form an inner set of tetrahedron walls that are surrounded by the outer four. The cage has significant interior volume, and was observed to bind anionic guests. The structure also possesses external binding clefts, located at the edges of the cage, which bound small aromatic guests. Halide ions bound to the silver clusters were observed to exchange in a well-defined hierarchy, allowing modulation of the cavity volume. The principles uncovered here may allow for increasingly more sophisticated cages with silver-cluster vertex architectures, with post-assembly tuning of the interior cavity volume enabling targeted binding behavior.

**M**etal-organic cages that assemble from metal ions and organic ligands possess well-defined interior cavities that can bind guests selectively. These molecular containers have applications in molecular recognition and chemical separations,<sup>[1]</sup> stabilization of highly reactive molecules,<sup>[2]</sup> catalysis,<sup>[3]</sup> and sensing.<sup>[4]</sup> Subcomponent self-assembly, whereby higher-order cage structures emerge from simple precursors through the simultaneous formation of covalent

$\text{C}=\text{N}$  and coordinative  $\text{N}\rightarrow\text{metal}$  coordination bonds, has allowed others<sup>[3d,5]</sup> and our group<sup>[1f,6]</sup> to prepare intricate three-dimensional structures, encompassing Platonic and Archimedean solids, and beyond.<sup>[7]</sup> Different design strategies produce architectures with different sizes and symmetries,<sup>[8]</sup> allowing tuning of the interior cavity size and properties.

The potential utility of  $\text{Ag}^{\text{I}}$  as a structural metal ion in such complex cages is highlighted by an elegant series of topologically entangled cages bound with silver(I) reported by Fujita and co-workers,<sup>[9]</sup> as well as a range of  $\text{Ag}^{\text{I}}$ -carbene cages and metallacycles.<sup>[10]</sup> The flexible coordination environment of  $\text{Ag}^{\text{I}}$  has also been used to synthesize a range of  $\text{Ag}^{\text{I}}$ -dipyridylpeptide coordination complexes, achieving even greater topological complexity.<sup>[11]</sup>

Self-assembled metal-organic structures that incorporate polymetallic clusters as vertices,<sup>[12]</sup> as opposed to single metal ions, are under development.<sup>[13]</sup> Strategies that enable the rational design of these more intricate assemblies are likewise under investigation. The ability of the 'soft' metal  $\text{Ag}^{\text{I}}$  to form clusters<sup>[14]</sup> and to support differing coordination numbers and environments makes this metal well suited to the formation of cluster-vertex assemblies.<sup>[15]</sup> We have reported a trigonal-prismatic structure containing disilver vertices,<sup>[16]</sup> and a series of hexameric helicates containing tetra- and hexa-silver clusters as vertices.<sup>[17]</sup> These structures demonstrate the diverse co-ordination environments that emerge when naphthyridine-imine ligands direct the formation of  $\text{Ag}^{\text{I}}$  clusters. However, previous structures provided relatively small internal volumes for guest binding.

[\*] S. E. Clark, Dr. A. W. Heard, Dr. C. T. McTernan, Dr. T. K. Ronson, Prof. J. R. Nitschke  
 Yusuf Hamied Department of Chemistry, University of Cambridge  
 Lensfield Road, Cambridge, CB2 1EW (UK)  
 E-mail: jrn34@cam.ac.uk

Dr. A. W. Heard  
 Astex Pharmaceuticals  
 436 Cambridge Science Park, Milton Road, Cambridge, CB4 0QA (UK)

Dr. C. T. McTernan  
 The Francis Crick Institute  
 Midland Road, London, NW1 1AT (UK)  
 and  
 Department of Chemistry, King's College London  
 7 Trinity Street, London, SE1 1DB (UK)

Dr. B. Rossi  
 Elettra Sincrotrone Trieste  
 Basovizza, 34149 Trieste (Italy)

P. Rozhin, Prof. S. Marchesan  
 Department of Chemical and Pharmaceutical Sciences, University of Trieste  
 Via Giorgieri 1, 34127 Trieste (Italy)  
 E-mail: smarchesan@units.it

Prof. S. Marchesan  
 Unit of Trieste,  
 INSTM  
 34127 Trieste (Italy)

[\*\*] A previous version of this manuscript has been deposited on a preprint server (<https://doi.org/10.26434/chemrxiv-2022-dkl3m>).

© 2023 The Authors. Angewandte Chemie International Edition published by Wiley-VCH GmbH. This is an open access article under the terms of the Creative Commons Attribution Non-Commercial NoDerivs License, which permits use and distribution in any medium, provided the original work is properly cited, the use is non-commercial and no modifications or adaptations are made.

In this work, we report the incorporation of  $[\text{Ag}_4\text{I}]^{3+}$  clusters into a previously unreported type of double-walled tetrahedral structure,<sup>[18]</sup> and explore its guest binding potential. This structure exhibits both interior and peripheral guest binding, with distinct groups of guests favoring each site. Furthermore, we found that the silver clusters at the tetrahedron vertices underwent halide exchange, which enabled us to tune the volume of the interior cavity.

The reaction between 1,3,5-tris(4-aminophenyl)benzene (**A**, 8 equiv) with 2-formyl-1,8-naphthyridine (**B**, 24 equiv),  $\text{Ag}^{\text{I}}$  bis(trifluoromethanesulfonyl)imide (triflimide,  $\text{NTf}_2^-$ , 16 equiv) and tetra-*n*-butylammonium iodide (TBAI, 4 equiv) produced cage **1** (Figure 1a). The  $^1\text{H}$  nuclear magnetic resonance (NMR) spectra of **1** exhibited two magnetically distinct ligand environments, with two distinct imine signals assigned by heteronuclear single quantum coherence spectroscopy (HSQC) (Figure S6). The diffusion ordered spectroscopy (DOSY) NMR spectrum confirmed that both environments corresponded to a single discrete structure, with a diffusion coefficient of  $3.06 \times 10^{-6} \text{ cm}^2 \text{ s}^{-1}$  in  $\text{CD}_3\text{CN}$ , giving a solvodynamic radius of 21.2 Å (Figure 1d). The mass spectrum (Figure S10–14) indicated a  $[\text{Ag}_{16}\text{I}_4\text{L}_8]^{12+}$  composition.

Single-crystal X-ray diffraction revealed the molecular structure of **1** to be a *T*-symmetric double-walled tetrahedron.<sup>[19]</sup> Two tritopic ligands span each face of the tetrahedron (Figure 1a), consistent with NMR and mass spectrometry. Each vertex consists of a  $[\text{Ag}_4\text{I}]^{3+}$  cluster (Figure 1c), with  $\text{Ag}^{\text{I}}\cdots\text{Ag}^{\text{I}}$  distances of 3.03 Å between the capping  $\text{Ag}^{\text{I}}$  and each of the three  $\text{Ag}^{\text{I}}$  centers closer to iodide. This distance is within the sum of the Van der Waals radii (3.44 Å) for two  $\text{Ag}^{\text{I}}$  ions, and similar to the 2.97–3.00 Å distance reported for previous vertex clusters<sup>[17]</sup> and other naphthyridine-bridged  $\text{Ag}^{\text{I}}$  clusters.<sup>[20]</sup> The phenyl cores of the inner and outer ligands are separated by 3.67 Å, in the typical range for an aromatic stacking interaction. The structure has a distance between farthest-spaced silver ions of 18.7 Å, comparable to the solvodynamic radius observed in DOSY. The innermost triads of  $\text{Ag}^{\text{I}}$  ions were separated by 4.32 Å, suggesting that these  $\text{Ag}^{\text{I}}$  ions do not undergo argentophilic interactions with each other.

Three observations help clarify how the naphthyridine-imine ligand binding groups help shape the silver clusters at the vertices of **1**. First, the imine nitrogen atoms of the inner panels (blue in Figure 1) are oriented away from the  $\text{Ag}^{\text{I}}$  centers, and are therefore uncoordinated. Second, the outer

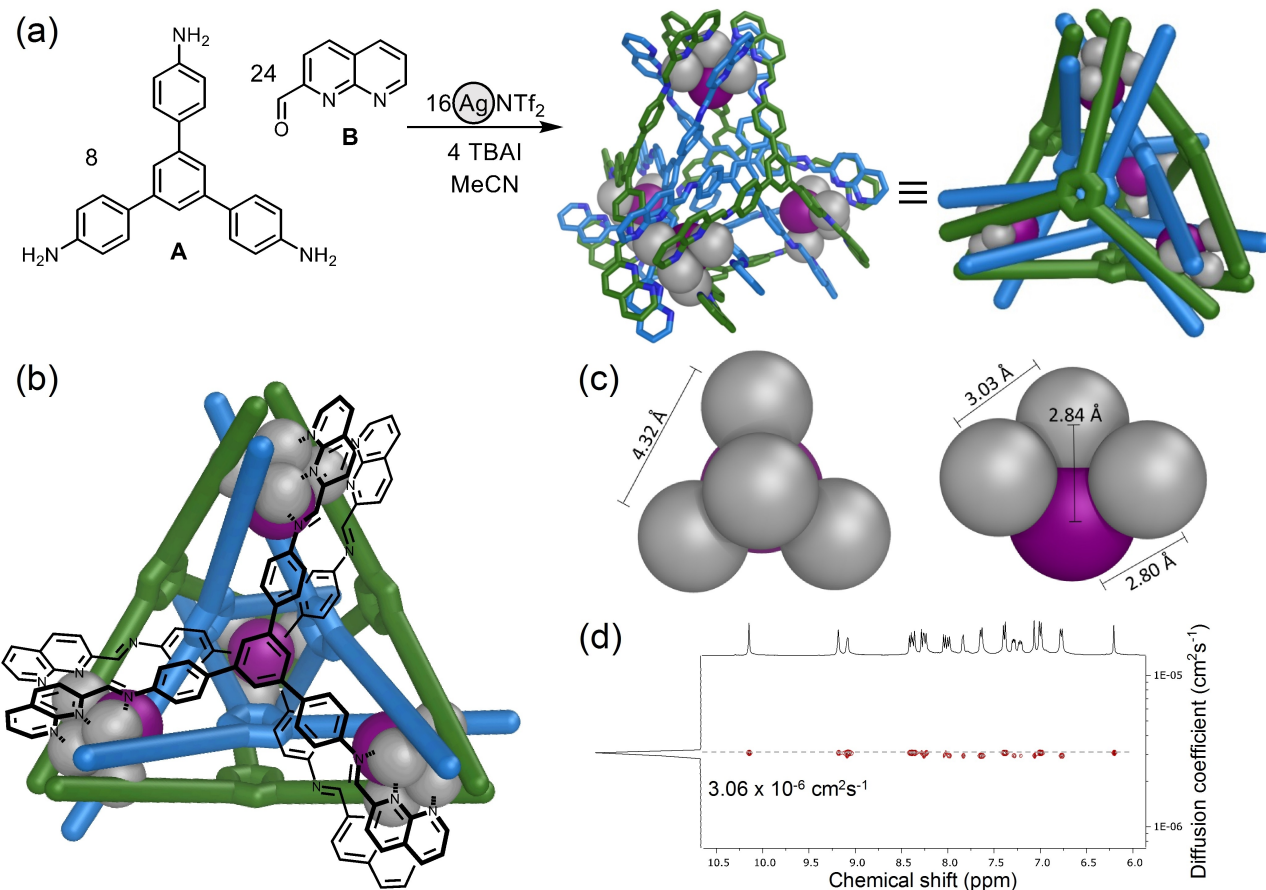


**Figure 1.** a) Self-assembly of subcomponents **A** and **B** with  $\text{Ag}^{\text{I}}\text{NTf}_2$  and TBAI, forming double-walled  $[\text{Ag}_{16}\text{I}_4\text{L}_8](\text{NTf}_2)_{12}$  tetrahedron **1**, showing two representations of the X-ray crystal structure of the cationic part of **1**. b) Coordination of ligand **L** in the inner and outer faces, with other ligands shown as cartoon representations. c) Detailed view of the structure of the  $[\text{Ag}_4\text{I}]^{3+}$  cluster, with  $\text{Ag}\cdots\text{Ag}$  and  $\text{Ag}\cdots\text{I}$  distances marked in Angstroms (Å). d)  $^1\text{H}$  DOSY NMR spectra of **1**.

ligands (green in Figure 1) adopt a bridging role, with each naphthyridine N-atom bound to a different  $\text{Ag}^{\text{I}}$  center (Figure 1b). Third, in contrast with these outer-ligand naphthyridines, one in each pair of naphthyridine N-atoms of the inner (blue) ligands effectively chelates  $\text{Ag}^{\text{I}}$  ions from the inner set closest to iodide. Each inner  $\text{Ag}^{\text{I}}$  thus coordinates to one naphthyridine nitrogen from an inner (blue) ligand and one from an outer (green) ligand. The flexibility of naphthyridine to either bridge or chelate  $\text{Ag}^{\text{I}}$  thus appears to again play an important role in bringing the silver-cluster vertices of **1** together, as has been observed elsewhere.<sup>[16,17,21]</sup>

The tight embrace of the tritopic ligands around the cage interior results in a high degree of enclosure. The available cavity space within **1** was calculated to be  $103 \text{ \AA}^3$  using Molovol.<sup>[22]</sup> With this available volume in mind, small neutral and anionic species were screened as potential guests for **1**.

In many cases, no change was observed in the NMR spectrum (Figure 2) upon adding the prospective guest to host **1**. The addition of anionic guests nitrate ( $\text{NO}_3^-$ ), periodate ( $\text{IO}_4^-$ ), bromate ( $\text{BrO}_3^-$ ), tetrafluoroborate ( $\text{BF}_4^-$ ), and perchlorate ( $\text{ClO}_4^-$ ) led to  $^1\text{H}$  NMR shifts of 0.04–0.10 ppm for the inward-facing imine  $^1\text{H}$  signal, with no shift observed for the externally-oriented imines (see Supporting Information, Section 8). This observation supports the assignment of interior binding ( $K_a = 2\text{--}9 \times 10^2 \text{ M}^{-1}$ , see Supporting Information Table S4), taking place in fast exchange on the NMR time scale. The volume of the anionic guests lay in the range  $41.1\text{--}67.7 \text{ \AA}^3$ ; all guests are of appropriate volume for the measured cavity volume of **1**.

Binding occurred with a 1:1 stoichiometry, as supported by a Job plot (Figure S67). We infer binding to be driven by coulombic interactions between the guests and the cationic  $\text{Ag}^{\text{I}}$  ions of the cage framework.

Small aromatic molecules were observed to bind externally to **1**. The presence of these guests (Figure 2) resulted in shifts to NMR signals of **1** assigned to the externally-oriented hydrogen atoms, as opposed to the internal ones observed to shift for anionic guests. For these prospective guests, binding was inferred to have taken place when chemical shifts changed by at least 0.04 ppm upon guest addition. A 2D rotating-frame nuclear Overhauser effect correlation spectroscopy (ROESY) NMR spectrum showed correlations between added benzene and  $^1\text{H}$  NMR signals assigned to hydrogen atoms at the tetrahedron edges (Figure S57), supporting the hypothesis that benzene binds at these sites. We thus infer that binding occurs externally with binding affinities of approximately  $2 \times 10^2 \text{ M}^{-1}$  (Supporting Information Table S4), involving aromatic stacking and van der Waals interactions between the guests and the large aromatic surface area exposed at the six edges of the tetrahedron cage **1**. A Job plot showed a clear maximum at a molar fraction of benzene at 0.85, supporting a 6:1 binding stoichiometry (Figure S66).<sup>[23]</sup> The assignment of this binding mode is further supported by the lack of NMR changes observed for larger aromatic prospective guests, such as naphthalene.

For many of the potential guests trialed, no evidence of binding was observed. We infer that non-planar, uncharged guests, such as hexane, tetrabromomethane, and neopentane do not engage in the aromatic stacking interactions of the

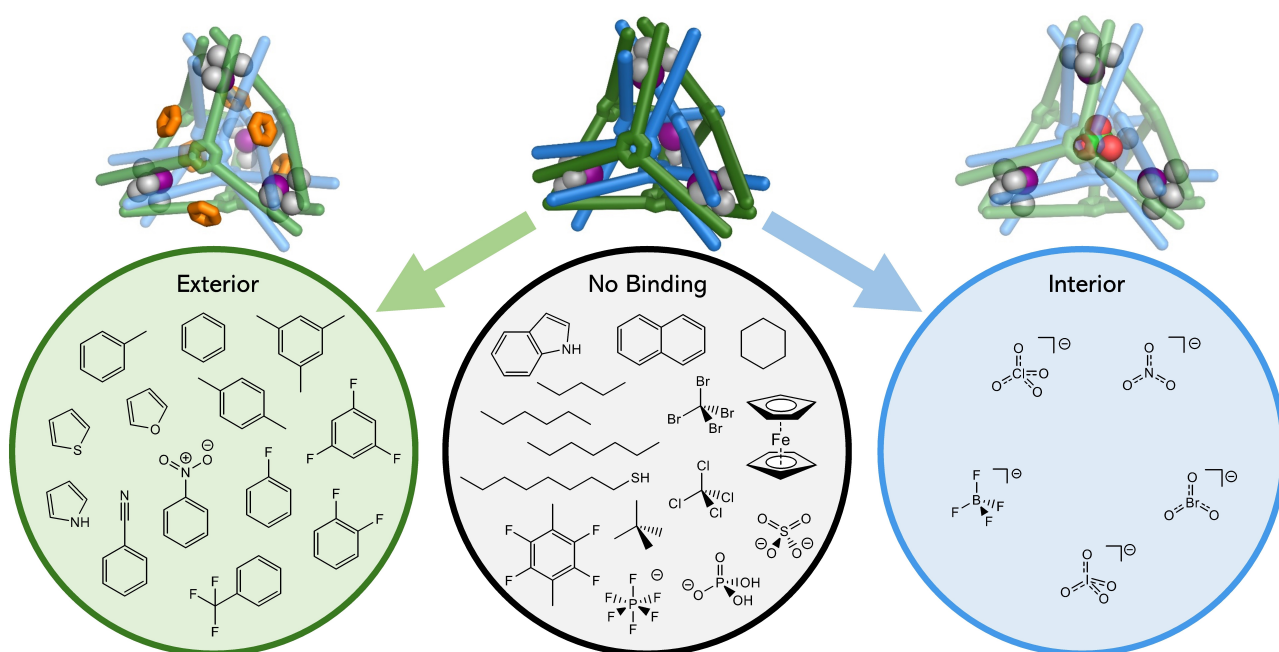


**Figure 2.** Schematic depicting the exterior (left) and interior (right) binding modes of double-walled tetrahedron **1**. The anionic guests bound within **1** are depicted in the blue circle at right. Small aromatic guests bound at the exterior of **1** are shown in the green circle at left. No binding was observed for the species shown in the central (black) circle.  $\text{BrO}_3^-$  was introduced as the potassium salt; all other anionic guests were used as the tetra-*n*-butylammonium salts.

exterior binding mode, nor do they benefit from an electrostatic driving force for encapsulation in the interior cavity. The presence of larger aromatic guests also caused no change in NMR spectra. We attribute this observation to the guest being too large for the external binding cleft. Three charged guests were also observed not to bind. In the case of  $\text{PF}_6^-$ , the guest is significantly larger than other interior binding guests, thus likely exceeding the upper size limit for interior binding. In the other two cases ( $\text{SO}_4^{2-}$  and  $\text{H}_2\text{PO}_4^-$ ) addition of the guest instead led to degradation of the cage.

Synthesis of **1** was repeated using other halides, such as TBAF, TBACl, and TBABr, in place of TBAI. While fluoride did not lead to clean assembly, the formation of analogs of **1** were observed with bromide (**2**) and chloride (**3**) as templating ions. The DOSY NMR spectra confirmed the formation of a similarly sized species, with two distinct ligand environments in the  $^1\text{H}$  NMR spectrum. Mass spectrometry confirmed the presence of the  $[\text{Ag}_{16}\text{X}_4\text{L}_8]-(\text{NTf}_2)_{12}$  species in solution.

We hypothesized that stronger binding between iodide and  $\text{Ag}^I$  could provide a driving force for halide exchange within the silver cluster. Such exchanges were observed to proceed, with a binding hierarchy of  $\text{I}^- > \text{Br}^- > \text{Cl}^-$ , shown in Figure 3. These processes were monitored by  $^1\text{H}$  NMR spectroscopy (Figures S43–48). These NMR spectra indicated the presence of intermediate species that incorporated two different halides, in slow exchange on the NMR time scale. Broadening of the  $^1\text{H}$  NMR spectra was observed alongside halide addition both in the case of halide exchange and excess of a lighter halide, attributed to possible aggregation or interior halide binding.

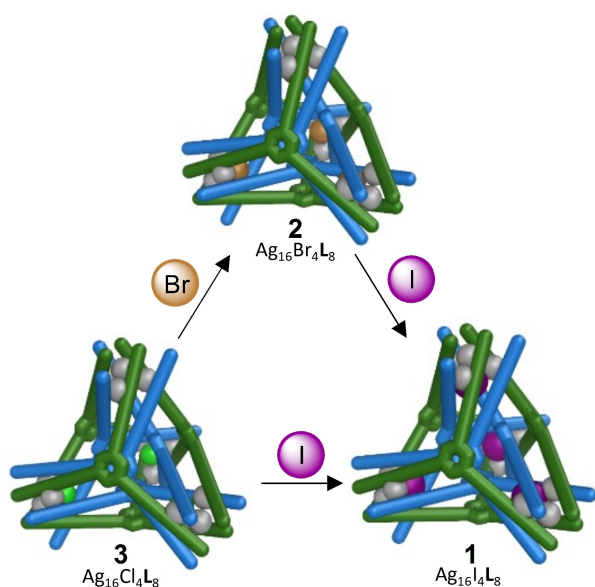


**Figure 3.** Successive halide exchange at the  $\text{Ag}_{16}$  clusters resulted in sequential transformations, allowing us to assign silver cluster halide affinity in the order  $\text{I}^- > \text{Br}^- > \text{Cl}^-$ . Halides were added as the tetra-*n*-butylammonium salts. See Supporting Information, Figure S43–48 for  $^1\text{H}$  NMR data.

Numerous attempts did not result in the isolation of single crystals of **2** or **3** with sufficient quality for X-ray analysis. However, modeling using the Scigress extended-MM3 method<sup>[24]</sup> with the crystal structure of **1** as a starting point allowed estimation of the differences in interior volume.<sup>[25]</sup> Analyses of the interiors in the modeled structures of cages **2** and **3** using Molovol<sup>[22]</sup> gave cavity volumes of  $111 \text{ \AA}^3$  and  $113 \text{ \AA}^3$  respectively.

Raman spectroscopy was used to verify the structure of cages **1–3** in thin films and in solution. Visible-light Raman spectra of thin films of cages **1–3** were dominated by signals arising from aromatic ligand coordination to the metal centers in the region  $1550\text{--}1650 \text{ cm}^{-1}$ .<sup>[26]</sup> Aniline signals were not observed, confirming the absence of cage hydrolysis (Figure S39). Evidence was observed for the presence of silver clusters in the region below  $500 \text{ cm}^{-1}$  (Figure S40). The  $\text{Ag}\cdots\text{Ag}$  distance of  $2.94 \text{ \AA}$  between the basal and apical  $\text{Ag}^I$  centers, obtained from the crystal structure of **1**, was used in conjunction with Herschbach–Laurie relationships<sup>[27]</sup> as implemented by Harvey et al.<sup>[28]</sup> From this relationship, a predicted  $\text{Ag}\cdots\text{Ag}$  force constant of  $0.236 \text{ mdyn \AA}^{-1}$  was obtained, which corresponds to a stretching frequency of  $86 \text{ cm}^{-1}$  (see Supporting Information page S35). Force constants determined this way have previously shown good agreement with experimentally determined Raman shifts.<sup>[27]</sup> While we were not able to observe the  $\text{Ag}\cdots\text{Ag}$  stretching band directly due to instrumental limits associated with Rayleigh rejection, the fundamental frequency was confirmed by two overtone peaks at  $323 \text{ cm}^{-1}$  and  $409 \text{ cm}^{-1}$ , with the corresponding spacing ( $\Delta\nu = 86 \text{ cm}^{-1}$ ) as previously reported for Ag clusters.<sup>[29]</sup>

Similar results were obtained for thin films of cages **2** and **3** ( $319\text{--}320 \text{ cm}^{-1}$ ,  $409 \text{ cm}^{-1}$ , Figure S40), corresponding to overtones of fundamental stretching bands at  $89\text{--}90 \text{ cm}^{-1}$ . This corresponds to a  $\text{Ag}\cdots\text{Ag}$  force constant of  $\approx 0.25 \text{ mdyn \AA}^{-1}$ , with a shorter  $\text{Ag}\cdots\text{Ag}$  distance consistent with  $\text{Ag}\text{--}\text{Br}$  and  $\text{Ag}\text{--}\text{Cl}$  bonding being weaker relative to  $\text{Ag}\text{--}\text{I}$ , and the atomic radii of Br and Cl being smaller than for I. These observations support our hypothesis that the cage framework remains unchanged upon substitution of the halide. Importantly, solution-state ultraviolet (UV) Resonance Raman measurements, performed at the Elettra synchrotron radiation facility using deep-UV excitation wavelength ( $\lambda = 266 \text{ nm}$ , Figure S41) close to the resonance of the aromatic moieties, resulted in the appearance of two signals at  $1587$  and  $1603 \text{ cm}^{-1}$ , likely resulting from non-covalent interactions between the double walls of the cage.

These Raman measurements thus provided evidence to support three conclusions. Firstly, that the double-walled cage framework persists in both the solid and solution states. Secondly, that subtle differences in  $\text{Ag}\cdots\text{Ag}$  stretching overtones report the presence of the different halides. Thirdly, that the ligands comprising the double walls of the cage are more mobile in solution than in the solid state. Absence of aniline peaks also confirmed cage integrity in solution. In the future, this spectroscopic approach may be useful for the structural characterization of cages for which single-crystal X-ray structure data are not available.

The structures of **1–3** thus add to the small set of known double-walled container molecules,<sup>[18,30]</sup> with the added unusual property of having identical ligands occupying both interior and exterior faces and the ability to bind guests in two distinct environments. The assembly of **1–3** was enabled by the remarkable ability of naphthyridine-imine ligands to support and shape silver(I) clusters. Analogous structures with extended ligands and thus the capacity to enclose larger guests may enable the design of chemical sensors, where luminescent silver cluster vertices<sup>[31]</sup> report on guest presence and identity.

## Acknowledgements

We thank Diamond Light Source (UK) for synchrotron beamtime on I19 (CY21497). S.E.C is the recipient of a PhD Studentship from BP through the BP International Centre for Advanced Materials (bp-ICAM). A.W.H. is the recipient of an Astex Pharmaceuticals Sustaining Innovation Post-Doctoral Award. C.T.M. thanks the Leverhulme Trust (ECF-2018-684), the Isaac Newton Trust, and Sidney Sussex College, Cambridge, for financial support. We acknowledge Elettra Sincrotrone Trieste for providing access to its synchrotron radiation facilities (proposal number 20220534) and networking support from COST Action CA17139 (eutopia.unitn.eu) funded by COST (www.cost.eu). This work was supported by the UK Engineering and Physical Sciences Research Council (EPSRC, and EP/T031603/1).

## Conflict of Interest

The authors declare no conflict of interest.

## Data Availability Statement

The data that support the findings of this study are available in the Supporting Information of this article.

**Keywords:** Metal Clusters · Metal-Organic Cages · Self-Assembly · Supramolecular Chemistry

[1] a) W. M. Bloch, Y. Abe, J. J. Holstein, C. M. Wandtke, B. Dittrich, G. H. Clever, *J. Am. Chem. Soc.* **2016**, *138*, 13750–13755; b) Z. Zhang, D. S. Kim, C.-Y. Lin, H. Zhang, A. D. Lammer, V. M. Lynch, I. Popov, O. Š. Miljanić, E. V. Anslyn, J. L. Sessler, *J. Am. Chem. Soc.* **2015**, *137*, 7769–7774; c) H. L. Ozores, M. Amorín, J. R. Granja, *J. Am. Chem. Soc.* **2017**, *139*, 776–784; d) R. Custelcean, P. V. Bonnesen, N. C. Duncan, X. Zhang, L. A. Watson, G. Van Berkel, W. B. Parson, B. P. Hay, *J. Am. Chem. Soc.* **2012**, *134*, 8525–8534; e) M. Yamashina, Y. Tanaka, R. Lavendomme, T. K. Ronson, M. Pittelkow, J. R. Nitschke, *Nature* **2019**, *574*, 511–515; f) D. Zhang, T. K. Ronson, Y.-Q. Zou, J. R. Nitschke, *Nat. Chem. Rev.* **2021**, *5*, 168–182; g) C. J. Bruns, D. Fujita, M. Hoshino, S. Sato, J. F. Stoddart, M. Fujita, *J. Am. Chem. Soc.* **2014**, *136*, 12027–12034; h) C. Fuertes-Espinosa, J. Murillo, M. E. Soto, M. R. Ceron, R.

Morales-Martínez, A. Rodríguez-Forteza, J. M. Poblet, L. Echegoyen, X. Ribas, *Nanoscale* **2019**, *11*, 23035–23041; i) S. Fang, W. Sun, C. Lin, F. Huang, H. Li, *Inorg. Chem.* **2023**, *62*, 1776–1780; j) Q. Li, Y. Wu, J. Cao, Y. Liu, Z. Wang, H. Zhu, H. Zhang, F. Huang, *Angew. Chem. Int. Ed.* **2022**, *61*, e202202381; *Angew. Chem.* **2022**, *134*, e202202381; k) A. Fuertes, M. Amorín, J. R. Granja, *Chem. Commun.* **2020**, *56*, 46–49; l) J.-L. Zhu, D. Zhang, T. K. Ronson, W. Wang, L. Xu, H.-B. Yang, J. R. Nitschke, *Angew. Chem. Int. Ed.* **2021**, *60*, 11789–11792; *Angew. Chem.* **2021**, *133*, 11895–11898.

[2] P. Mal, B. Breiner, K. Rissanen, J. R. Nitschke, *Science* **2009**, *324*, 1697–1699.

[3] a) M. Yoshizawa, M. Tamura, M. Fujita, *Science* **2006**, *312*, 251–254; b) C. M. Hong, R. G. Bergman, K. N. Raymond, F. D. Toste, *Acc. Chem. Res.* **2018**, *51*, 2447–2455; c) D. M. Kaphan, M. D. Levin, R. G. Bergman, K. N. Raymond, F. D. Toste, *Science* **2015**, *350*, 1235–1238; d) W. Cullen, M. C. Misuraca, C. A. Hunter, N. H. Williams, M. D. Ward, *Nat. Chem.* **2016**, *8*, 231–236; e) P. Howlader, P. Das, E. Zangrando, P. S. Mukherjee, *J. Am. Chem. Soc.* **2016**, *138*, 1668–1676; f) Y. Fang, J. A. Powell, E. Li, Q. Wang, Z. Perry, A. Kirchon, X. Yang, Z. Xiao, C. Zhu, L. Zhang, F. Huang, H. C. Zhou, *Chem. Soc. Rev.* **2019**, *48*, 4707–4730; g) D. Chu, W. Gong, H. Jiang, X. Tang, Y. Cui, Y. Liu, *CCS Chem.* **2022**, *4*, 1180–1189; h) F. F. Chu, L.-J. Chen, S. Chen, G.-Y. Wu, W.-L. Jiang, J.-C. Shen, Y. Qin, L. Xu, H.-B. Yang, *Chem* **2020**, *6*, 2395–2406; i) E. Ubasart, O. Borodin, C. Fuertes-Espinosa, Y. Xu, C. García-Simón, L. Gómez, J. Juanhuix, F. Gándara, I. Imaz, D. MasPOCH, M. von Delius, X. Ribas, *Nat. Chem.* **2021**, *13*, 420–427; j) J. Jökel, F. Schwer, M. von Delius, U.-P. Apfel, *Chem. Commun.* **2020**, *56*, 14179–14182.

[4] a) K. Wu, K. Li, Y.-J. Hou, M. Pan, L.-Y. Zhang, L. Chen, C.-Y. Su, *Nat. Commun.* **2016**, *7*, 10487; b) W. Xue, T. K. Ronson, Z. Lu, J. R. Nitschke, *J. Am. Chem. Soc.* **2022**, *144*, 6136–6142; c) M. Denis, L. Qin, P. Turner, K. A. Jolliffe, S. M. Goldup, *Angew. Chem. Int. Ed.* **2018**, *57*, 5315–5319; *Angew. Chem.* **2018**, *130*, 5413–5417; d) M. Denis, J. Pancholi, K. Jobe, M. Watkinson, S. M. Goldup, *Angew. Chem. Int. Ed.* **2018**, *57*, 5310–5314; *Angew. Chem.* **2018**, *130*, 5408–5412; e) J. Pancholi, D. J. Hodson, K. Jobe, G. A. Rutter, S. M. Goldup, M. Watkinson, *Chem. Sci.* **2014**, *5*, 3528–3535; f) K. Jobe, C. H. Brennan, M. Motevalli, S. M. Goldup, M. Watkinson, *Chem. Commun.* **2011**, *47*, 6036.

[5] a) R.-J. Li, A. Tarzia, V. Posligua, K. E. Jelfs, N. Sanchez, A. Marcus, A. Baksi, G. H. Clever, F. Fadaei-Tirani, K. Severin, *Chem. Sci.* **2022**, *13*, 11912–11917; b) W. Li, C. Liu, J. Kfoury, J. Oláh, K. Robeyns, M. L. Singleton, S. Demeshko, F. Meyer, Y. Garcia, *Chem. Commun.* **2022**, *58*, 11653–11656; c) Y. Lei, Q. Chen, P. Liu, L. Wang, H. Wang, B. Li, X. Lu, Z. Chen, Y. Pan, F. Huang, H. Li, *Angew. Chem. Int. Ed.* **2021**, *60*, 4705–4711; *Angew. Chem.* **2021**, *133*, 4755–4761.

[6] a) C. T. McTernan, J. A. Davies, J. R. Nitschke, *Chem. Rev.* **2022**, *122*, 10393–10437; b) D. Zhang, T. K. Ronson, J. R. Nitschke, *Acc. Chem. Res.* **2018**, *51*, 2423–2436.

[7] a) J. P. Carpenter, C. T. McTernan, J. L. Greenfield, R. Lavendomme, T. K. Ronson, J. R. Nitschke, *Chem* **2021**, *7*, 1534–1543; b) J. A. Davies, T. K. Ronson, J. R. Nitschke, *Chem* **2022**, *8*, 1099–1106; c) T. K. Ronson, Y. Wang, K. Baldrige, J. S. Siegel, J. R. Nitschke, *J. Am. Chem. Soc.* **2020**, *142*, 10267–10272; d) L. Xu, Y.-X. Wang, L.-J. Chen, H.-B. Yang, *Chem. Soc. Rev.* **2015**, *44*, 2148–2167; e) Z. Liu, Z. Tian, W. Li, S. Meng, L. Wang, J. Ma, *J. Org. Chem.* **2012**, *77*, 8124–8130; f) Y. Xu, S. Gsänger, M. B. Minameyer, I. Imaz, D. MasPOCH, O. Shyshov, F. Schwer, X. Ribas, T. Drewello, B. Meyer, M. von Delius, *J. Am. Chem. Soc.* **2019**, *141*, 18500–18507.

[8] a) T. R. Cook, P. J. Stang, *Chem. Rev.* **2015**, *115*, 7001–7045; b) A. J. McConnell, *Chem. Rev.* **2022**, *51*, 2957–2971; c) A.

- Tarzia, K. E. Jelfs, *Chem. Commun.* **2022**, 58, 3717–3730; d) D. Fujita, Y. Ueda, S. Sato, N. Mizuno, T. Kumasaka, M. Fujita, *Nature* **2016**, 540, 563–566; e) A. Takai, T. Kajitani, T. Fukushima, K. Kishikawa, T. Yasuda, M. Takeuchi, *J. Am. Chem. Soc.* **2016**, 138, 11245–11253; f) S. Ogi, V. Stepanenko, K. Sugiyasu, M. Takeuchi, F. Würthner, *J. Am. Chem. Soc.* **2015**, 137, 3300–3307; g) N. Sasaki, M. F. J. Mabeoone, J. Kikkawa, T. Fukui, N. Shioya, T. Shimoaka, T. Hasegawa, H. Takagi, R. Haruki, N. Shimizu, S. Adachi, E. W. Meijer, M. Takeuchi, K. Sugiyasu, *Nat. Commun.* **2020**, 11, 3578; h) G. M. Lang, T. Shima, L. Wang, K. J. Cluff, K. Skopek, F. Hampel, J. Blümel, J. A. Gladysz, *J. Am. Chem. Soc.* **2016**, 138, 7649–7663; i) A. L. Estrada, L. Wang, G. Hess, F. Hampel, J. A. Gladysz, *Inorg. Chem.* **2022**, 61, 17012–17025.
- [9] a) Y. Domoto, M. Abe, K. Yamamoto, T. Kikuchi, M. Fujita, *Chem. Sci.* **2020**, 11, 10457–10460; b) Y. Domoto, M. Abe, T. Kikuchi, M. Fujita, *Angew. Chem. Int. Ed.* **2020**, 59, 3450–3454; *Angew. Chem.* **2020**, 132, 3478–3482; c) Y. Domoto, M. Abe, M. Fujita, *J. Am. Chem. Soc.* **2021**, 143, 8578–8582; d) Y. Domoto, K. Yamamoto, S. Horie, Z. Yu, M. Fujita, *Chem. Sci.* **2022**, 13, 4372–4376.
- [10] a) D. Wang, B. Zhang, C. He, P. Wu, C. Duan, *Chem. Commun.* **2010**, 46, 4728; b) L. Zhang, R. Das, C. Li, Y. Wang, F. E. Hahn, K. Hua, L. Sun, Y. Han, *Angew. Chem. Int. Ed.* **2019**, 58, 13360–13364; *Angew. Chem.* **2019**, 131, 13494–13498; c) Y.-W. Zhang, S. Bai, Y.-Y. Wang, Y.-F. Han, *J. Am. Chem. Soc.* **2020**, 142, 13614–13621.
- [11] a) T. Sawada, A. Saito, K. Tamiya, K. Shimokawa, Y. Hisada, M. Fujita, *Nat. Commun.* **2019**, 10, 921; b) Y. Inomata, T. Sawada, M. Fujita, *Chem* **2020**, 6, 294–303; c) J. E. M. Lewis, *Chem* **2020**, 6, 14–15; d) Y. Inomata, T. Sawada, M. Fujita, *J. Am. Chem. Soc.* **2021**, 143, 16734–16739; e) T. Sawada, M. Fujita, *Bull. Chem. Soc. Jpn.* **2021**, 94, 2342–2350.
- [12] a) M. Bera, G. Aromi, W. T. Wong, D. Ray, *Chem. Commun.* **2006**, 671; b) S.-K. Peng, H. Yang, D. Luo, M. Xie, W.-J. Tang, G.-H. Ning, D. Li, *Inorg. Chem. Front.* **2022**, 9, 5327–5334; c) Y. Wu, M. Xie, J.-K. Jin, Z.-Y. Zhang, H. Hu, Y.-P. Tian, Y.-Q. Xiao, G.-H. Ning, D. Li, X. Jiang, *Small Struct.* **2022**, 3, 2100155.
- [13] a) L. J. Wang, S. Bai, Y. F. Han, *J. Am. Chem. Soc.* **2022**, 144, 16191–16198; b) A. Sarwa, A. Białońska, M. Garbicz, B. Szyszko, *Chem. Eur. J.* **2023**, 29, e202203850.
- [14] a) H. Kwon, E. Pietrasiak, T. Ohhara, A. Nakao, B. Chae, C.-C. Hwang, D. Jung, I.-C. Hwang, Y. H. Ko, K. Kim, E. Lee, *Inorg. Chem.* **2021**, 60, 6403–6409; b) S. Horiuchi, S. Moon, A. Ito, J. Tessarolo, E. Sakuda, Y. Arikawa, G. H. Clever, K. Umakoshi, *Angew. Chem. Int. Ed.* **2021**, 60, 10654–10660; *Angew. Chem.* **2021**, 133, 10749–10755; c) M. Cuerva, R. García-Fandiño, C. Vázquez-Vázquez, M. A. López-Quintela, J. Montenegro, J. R. Granja, *ACS Nano* **2015**, 9, 10834–10843.
- [15] J. Zhang, M. Nieuwenhuyzen, J. P. H. Charmant, S. L. James, *Chem. Commun.* **2004**, 2808.
- [16] J. P. Carpenter, C. T. McTernan, T. K. Ronson, J. R. Nitschke, *J. Am. Chem. Soc.* **2019**, 141, 11409–11413.
- [17] C. T. McTernan, T. K. Ronson, J. R. Nitschke, *J. Am. Chem. Soc.* **2021**, 143, 664–670.
- [18] Y. Tamura, H. Takezawa, M. Fujita, *J. Am. Chem. Soc.* **2020**, 142, 5504–5508.
- [19] Deposition number 2215164 contains the supplementary crystallographic data for this paper. These data are provided free of charge by the joint Cambridge Crystallographic Data Centre and Fachinformationszentrum Karlsruhe Access Structures service.
- [20] T. Tsuda, S. Ohba, M. Takahashi, M. Ito, *Acta Crystallogr. Sect. C* **1989**, 45, 887–890.
- [21] a) G.-H. Niu, H. C. Wentz, S.-L. Zheng, M. G. Campbell, *Inorg. Chem. Commun.* **2019**, 101, 142–144; b) A. N. Desnoyer, A. Nicolay, P. Rios, M. S. Ziegler, T. D. Tilley, *Acc. Chem. Res.* **2020**, 53, 1944–1956.
- [22] J. B. Maglic, R. Lavendomme, *J. Appl. Crystallogr.* **2022**, 55, 1033–1044.
- [23] D. Brynn Hibbert, P. Thordarson, *Chem. Commun.* **2016**, 52, 12792–12805.
- [24] N. L. Allinger, Y. H. Yuh, J. H. Lii, *J. Am. Chem. Soc.* **1989**, 111, 8551–8566.
- [25] **Note:** Geometry optimized structures were modelled using the MM3 force field on SCIGRESS software (Fujitsu Limited, Tokyo, Japan, 2013) Version FJ 2.6 (EU 3.1.9) Build 5996.8255.20141202., 2013.
- [26] M. Kieffer, A. M. Garcia, C. J. E. Haynes, S. Kralj, D. Iglesias, J. R. Nitschke, S. Marchesan, *Angew. Chem. Int. Ed.* **2019**, 58, 7982–7986; *Angew. Chem.* **2019**, 131, 8066–8070.
- [27] D. R. Herschbach, V. W. Laurie, *J. Chem. Phys.* **1961**, 35, 458–464.
- [28] a) D. Perreault, M. Drouin, A. Michel, P. D. Harvey, *Inorg. Chem.* **1993**, 32, 1903–1912; b) P. Harvey, *Coord. Chem. Rev.* **1996**, 153, 175–198.
- [29] K. A. Bosnick, PhD thesis, University of Toronto (Canada), **2000**.
- [30] a) X. Zhao, H. Wang, B. Li, W. Zhang, X. Li, W. Zhao, C. Janiak, A. W. Heard, X. Yang, B. Wu, *Angew. Chem. Int. Ed.* **2022**, 61, e202115042; *Angew. Chem.* **2022**, 134, e202115042; b) M. Tang, Y. Liang, X. Lu, X. Miao, L. Jiang, J. Liu, L. Bian, S. Wang, L. Wu, Z. Liu, *Chem* **2021**, 7, 2160–2174.
- [31] M.-M. Zhang, X.-Y. Dong, Z.-Y. Wang, X.-M. Luo, J.-H. Huang, S.-Q. Zang, T. C. W. Mak, *J. Am. Chem. Soc.* **2021**, 143, 6048–6053.

Manuscript received: February 1, 2023

Accepted manuscript online: February 23, 2023

Version of record online: March 13, 2023